Chem

CellPress

Article

Reinforced double-threaded slide-ring networks for accelerated hydrogel discovery and 3D printing

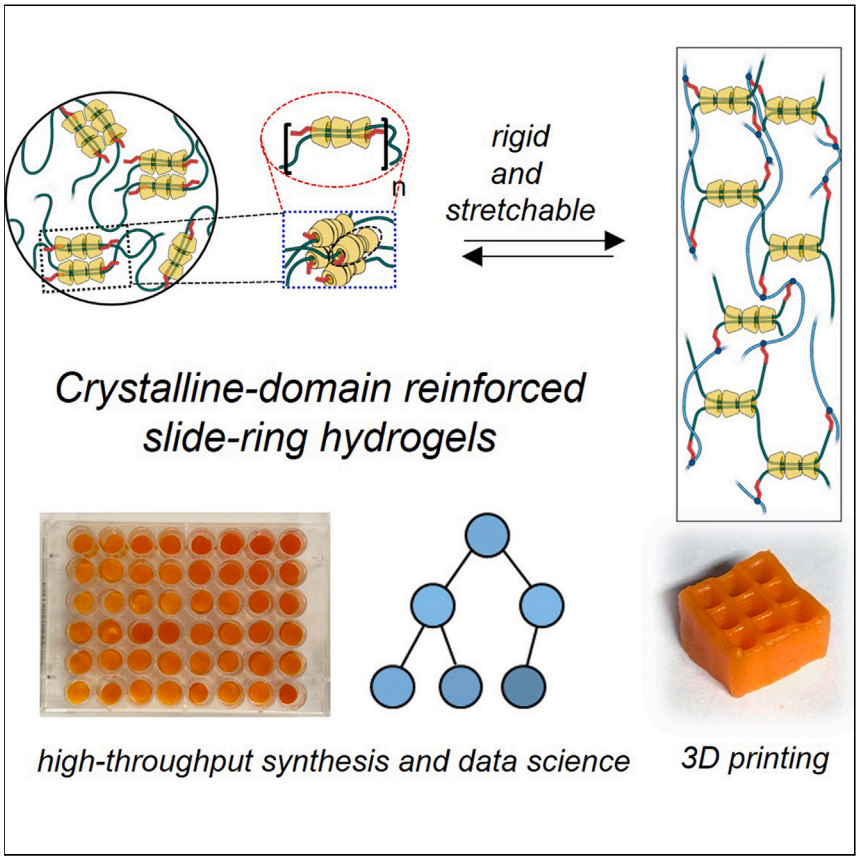

Ke and co-workers have designed a crystalline-domain-reinforced double-threaded slide-ring network to surpass the elasticity-toughness trade-off in conventional slide-ring gels. They employ 3D-printable modular crosslinkers that feature rigid crystalline domains and mobile γ-cyclodextrin slide-ring joints to create slide-ring hydrogels. The efficient, high-throughput production of these hydrogels, combined with data-science-facilitated structure-property elucidation, has led to the identification of superior slide-ring gels suitable for 3D printing and the fabrication of capacitive stress sensors.

Miao Tang, Dan Zheng, Jayanta Samanta, Esther H.R. Tsai, Huibin Qiu, Jacquelyne A. Read, Chenfeng Ke

jacquelyne.a.read@dartmouth.edu (J.A.R.)
chenfeng.ke@dartmouth.edu (C.K.)

Highlights

Crystalline-domain-reinforced double-threaded slide-ring gels are introduced

A modular crosslinker is employed for synthesizing rigid and stretchable slide-ring gels

High-throughput synthesis is used for creating a library of slide-ring gels

The hydrogels are used for 3D printing high-performance capacitive stress sensors

Tang et al., Chem 9, 1–17
December 14, 2023
https://doi.org/10.1016/j.chempr.2023.07.020

Please cite this article in press as: Tang et al., Reinforced double-threaded slide-ring networks for accelerated hydrogel discovery and 3D printing, Chem (2023), https://doi.org/10.1016/j.chempr.2023.07.020

Chem

CellPress

Article

Reinforced double-threaded slide-ring networks for accelerated hydrogel discovery and 3D printing

Miao Tang,[1] Dan Zheng,[1] Jayanta Samanta,[1] Esther H.R. Tsai,[2] Huibin Qiu,[3] Jacquelyne A. Read,[1,*] and Chenfeng Ke[1,4,*]

SUMMARY

Traditionally, slide-ring gels are stretchable but soft as a result of an elasticity-stretchability trade-off. Herein, we introduce a new approach to breaking this trade-off and creating reinforced slide-ring networks with mobile crosslinkers. Our approach involves the construction of a polyethylene glycol double-threaded γ-cyclodextrin-based pro-slide-ring crosslinker that serves as a modular component for 3D printing and copolymerization. The resulting crystalline-domain-reinforced slide-ring hydrogels, or CrysDoS-gels, exhibit both high elasticity and high stretchability. The modular synthesis allows for high-throughput synthesis of CrysDoS-gels, generating a large amount of data for structure-property analysis. By employing data science techniques, such as machine learning and linear regression, not only were we able to identify which chemical components influence the mechanical properties of CrysDoS-gels, but this analysis also aided in the discovery of better-performing CrysDoS-gels. Finally, we demonstrate the potential application of the newly discovered CrysDoS-gels as sensing devices by 3D printing them as stress sensors with high sensitivity and a broad detection range.

INTRODUCTION

Synthetic polymer-based hydrogels have been extensively exploited for biomedical,[1] pharmaceutical,[2,3] and mechanical engineering[4,5] because of their biocompatibility, high water content, and tunable chemical and physical properties.[6] Currently, various hydrogels with different mechanical properties have been synthesized through molecular designs tailored to meet the requirements of the deploying environment. For example, hydrogels designed for contact lenses must be soft and less swellable and have been synthesized as covalently crosslinked polymer networks.[7] Calcium alginate dressings used for wound healing are formed by the physical crosslinking of alginate with calcium ions and are designed to swell to speed wound homeostasis.[8] However, the rapidly expanding demands for hydrogels greatly exceed the chemical and physical properties that conventional hydrogels can offer. Hence, extensive fundamental efforts have been made to design and synthesize polymers with advanced network architectures.[9,10] One example of such an architecture is the double network (or interpenetrated network) introduced by Gong et al.; in this network, one dissipative polymer network is infused into another dissimilar polymer network.[11] As a result of the double-network design, strong and stretchable hydrogels have been developed.[12,13]

Another breakthrough, made by Ito and co-workers, is the development of slide-ring gels with mobile crosslinkers (Figure 1A).[14,15] In these slide-ring gels, polymers are

THE BIGGER PICTURE

Stretchable slide-ring hydrogels are typically soft because of an elasticity-toughness trade-off. Herein, we have developed crystalline-domain-reinforced double-threaded slide-ring networks by introducing a pro-slide-ring crosslinker synthesized through the self-assembly of γ-cyclodextrins and telechelic polyethylene glycols. We obtained 3D-printable rigid and tough slide-ring hydrogels. The modular reactivity of the pro-slide-ring crosslinker enables a high-throughput synthesis, resulting in a library of slide-ring hydrogels with varying mechanical properties. We illustrate the structure-property relationships of these hydrogels by using data science tools, leading to the discovery of superior hydrogels. We fabricated a high-performance 3D-printed stress sensor to show the potential of this design. Introducing a modular pro-slide-ring crosslinker with a clearly illustrated structure-property relationship greatly accelerates the discovery of mechanically robust slide-ring-based soft materials.

Please cite this article in press as: Tang et al., Reinforced double-threaded slide-ring networks for accelerated hydrogel discovery and 3D printing, Chem (2023), https://doi.org/10.1016/j.chempr.2023.07.020

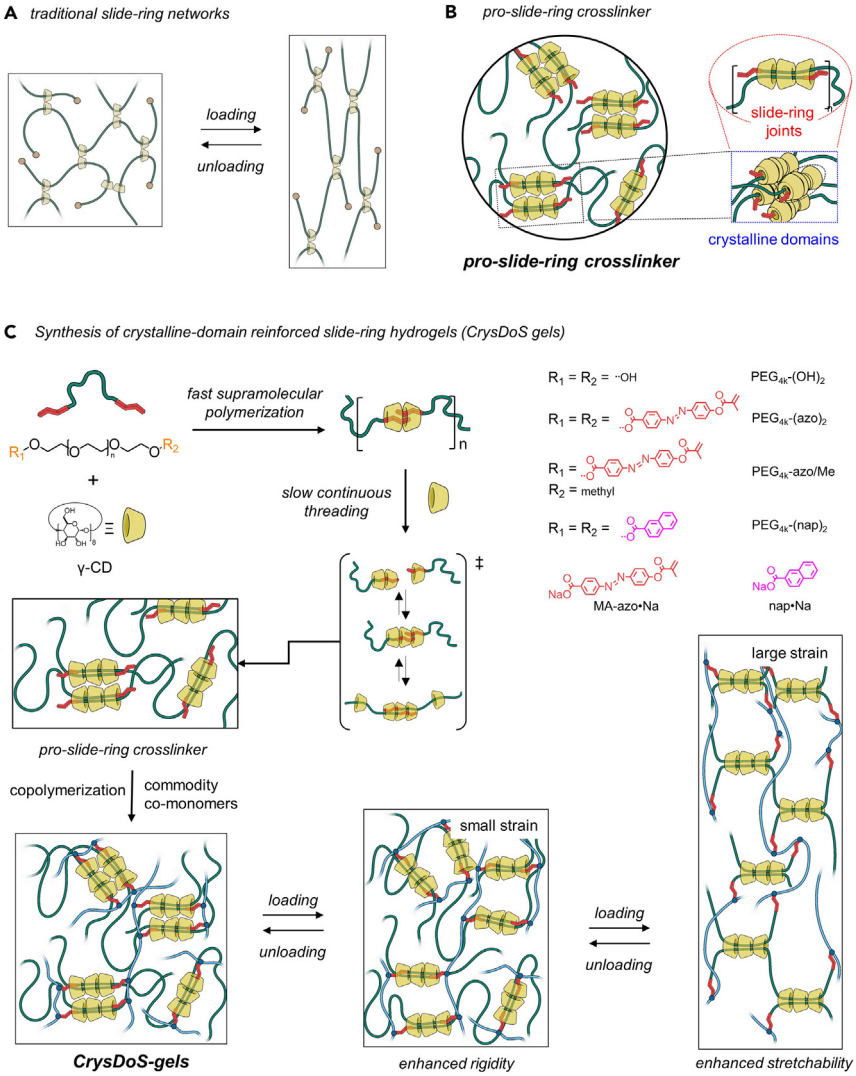

Figure 1. Development of crystalline-domain-reinforced 3D-printable double-threaded slide-ring hydrogels (CrysDoS-gels)

(A) A traditional stretchable slide-ring gel.

(B) Cartoon representation of a pro-slide-ring crosslinker with crystalline domains and dormant slide-ring joints.

(C) CrysDoS-gels synthesized by copolymerization of the pro-slide-ring crosslinker and co-monomers. The CrysDoS hydrogel undergoes two-stage deformations via disruption of the crystalline domain followed by the γ-CD sliding.

connected by a pair of covalently linked α-cyclodextrins (α-CDs) sliding along the polymer chain.[14–16] Slide-ring gels feature a mechano-adaptive network in which the mobile crosslinkers reorganize themselves in response to the external mechanical force.[17] Slide-ring gels with mobile crosslinkers exhibit exceptional stretchability and high toughness, making them attractive for applications requiring high stretchability, toughness, and recoverability. For instance, when slide-ring networks are integrated with batteries,[18] elastomers,[19] and 3D-printed hydrogels,[20] the mechanical properties of the materials are significantly improved. However, they tend to be soft because the activation energy required for ring-pair sliding is low,[21] resulting in an elasticity-toughness trade-off in the current slide-ring gel design.

[1]Department of Chemistry, Dartmouth College, Hanover, NH 03755, USA

[2]Center for Functional Nanomaterials, Brookhaven National Laboratory, Upton, NY 11973, USA

[3]School of Chemistry and Chemical Engineering, Shanghai Jiao Tong University, Shanghai 200240, China

[4]Lead contact

*Correspondence: jacquelyne.a.read@dartmouth.edu (J.A.R.), chenfeng.ke@dartmouth.edu (C.K.)

https://doi.org/10.1016/j.chempr.2023.07.020

Please cite this article in press as: Tang et al., Reinforced double-threaded slide-ring networks for accelerated hydrogel discovery and 3D printing, Chem (2023), https://doi.org/10.1016/j.chempr.2023.07.020

Therefore, it is of utmost importance to explore new chemical approaches that can break the trade-off between low elasticity and high toughness in slide-ring gels. Such advances would expand their potential applications to materials such as scratch-proof coatings[19] and robust electronic skins.[22] The challenge is to reinforce the slide-ring networks while still preserving the mobility of the dynamic crosslinkers. Moreover, it is imperative to create modular pro-slide-ring crosslinkers that can be easily converted into slide-ring networks in one step through copolymerization with commodity monomers, akin to how prochiral compounds can be transformed into chiral products in a single step. With a facile and modular synthesis, the discovery of slide-ring crosslinked materials of diverse mechanical properties could be greatly accelerated.

In response to the challenges of discovering mechanically robust slide-ring networks, we introduce a new approach that utilizes modular crystalline-domain-reinforced pro-slide-ring crosslinkers to accelerate the process. These modular crosslinkers are suitable for direct-ink-writing (DIW) 3D printing and enable high-throughput synthesis because of their rapid gelation and excellent viscoelasticity. A typical pro-slide-ring crosslinker is a supramolecular polymer formed by double-threaded polyethylene glycols (PEGs) in γ-CDs (Figure 1B), which can react with various co-monomers to form slide-ring networks (Figure 1C). The modular reactivity and excellent viscoelasticity of pro-slide-ring crosslinkers enable high-throughput synthesis and 3D printing. As such, we were able to obtain a sizable library of hydrogel materials with various elastic moduli, compressibility, and viscoelasticity through high-throughput synthesis. Among these materials, we have identified a group of hydrogels that exhibit high elasticity and toughness, breaking the elasticity-toughness trade-off in conventional slide-ring networks and facilitating additional 3D printability. This library of CrysDoS-gels also enabled us to leverage machine-learning methods and multivariate linear regression techniques to identify structure-property relationships and discover better materials. We then fabricated these hydrogels as capacitive stress sensors, which exhibited both high sensitivity and a broad range of detection, through multi-material 3D printing.

RESULTS

Slide-ring gels with mobile crosslinkers are typically synthesized in solution through either the crosslinking of two α-CDs on different polyrotaxanes[14] (Figure 1A) or the copolymerization of acrylate monomers with vinyl-α-CD-threaded polyrotaxanes.[19,23] To achieve stretchable slide-ring gels, the hydroxyls of α-CDs are substituted to prevent inter-α-CD hydrogen bonding.[16,23] Otherwise, α-CD aggregations can hinder their free sliding along the axle to limit the mobility of the crosslinker. These factors render these slide-ring gels stretchable but soft. Alternatively, γ-CD is known to accommodate two PEG axles in its cavity to form doubly threaded assemblies.[24–26] The dual threading of PEG axles inside γ-CD could be promoted by the installation of aromatic end groups to PEG for the formation of a ternary complex.[24,27,28] When γ-CDs are used for the construction of networks with double-threaded mobile junctions, the yielded slide-ring gels remain soft.[29–32] Moreover, to maximize the translocation distances for mobile crosslinkers, fewer modified α-CDs or γ-CDs per axle are desirable, but controlling the number of threaded CDs through synthetic modulation[15,16,33] remains a challenge.

To overcome these challenges, we opted for γ-CD as the mobile ring crosslinker to construct stretchable and rigid slide-ring networks by capitalizing on the kinetically formed crystalline γ-CD aggregates. We designed two PEG axles, PEG_{4k}-$(azo)_2$ and

Please cite this article in press as: Tang et al., Reinforced double-threaded slide-ring networks for accelerated hydrogel discovery and 3D printing, Chem (2023), https://doi.org/10.1016/j.chempr.2023.07.020

PEG_{4k}-$(nap)_2$ (M_n of 4 kDa), whose end groups are known to form 2:1 or 2:2 complexes with γ-CD (Figure 1C). When γ-CDs are mixed with PEG_{4k}-$(azo)_2$, γ-CD-connected supramolecular polymers form rapidly. The high-affinity $(azo)_2$•γ-CD inclusion complexes formed at the joints of the supramolecular polymer not only limit the continuous γ-CD threading but also trigger a kinetically accelerated crystallization process at room temperature, affording the pro-slide-ring crosslinker (Figure 1C).

Three PEG axles—PEG_{4k}-$(azo)_2$, PEG_{4k}-azo/Me, and PEG_{4k}-$(nap)_2$—were synthesized by end-group esterification (Figure 1C). The corresponding model compounds of these end groups, which include MA-azo•Na, 4′-hydroxy azobenzene-4-carboxylic acid (azo-CO_2H), and nap•Na, were also prepared for the investigation. Job plots (Figure 2A) suggested that both MA-azo•Na and nap•Na form *n*:*n* inclusion complexes with γ-CDs. The binding stoichiometries of these inclusion complexes were confirmed as 2:2 complexes $(MA\text{-}azo)_2$•$(\gamma\text{-}CD)_2$ and $(nap)_2$•$(\gamma\text{-}CD)_2$ through NMR experiments (supplemental experimental procedures section S2) and single-crystal X-ray structure analysis of the $(azo\text{-}CO_2H)_2$•$(\gamma\text{-}CD)_2$ complex (Figure 2B). The binding affinities between a pair of MA-azo•Na and γ-CD were measured as $K_1 = (1.8 \pm 0.2) \times 10^4\ M^{-1}$ and $K_2 = (1.7 \pm 0.1) \times 10^3\ M^{-1}$ via ^1H NMR titration at 298 K (Figure S7).[34] Similarly, the binding affinities between a pair of nap•Na and γ-CD were measured as $K_1 = 180 \pm 1\ M^{-1}$ and $K_2 = 5.0 \pm 0.1\ M^{-1}$ (Figure S8).

Compared with those of MA-azo•Na, the proton resonances of the MA-azo•γ-CD 2:2 complex shifted upfield as a result of shielding of the neighboring co-included MA-azo (Figure 2C, i and ii). Similar shifts were also observed in a 1:1 mixture of PEG_{4k}-azo/Me and γ-CD in D_2O and a 1:1 mixture of PEG_{4k}-$(azo)_2$ and γ-CD in D_2O (Figure 2C, iv and v), confirming the formation of 2:2 complexes between γ-CDs and the end groups of these PEG axles. 1D and 2D nuclear Overhauser effect (NOE) experiments revealed that these azobenzene end groups were co-threaded from opposite directions (Figure S11) and generated linear supramolecular polymers in the solution. ^1H NMR studies of the 1:1 mixture of PEG_{4k}-$(nap)_2$ and γ-CD showed similar phenomena (Figure S12).

In the presence of an excess of γ-CD, PEG axles are known to form double PEG-threaded polypseudorotaxanes and crystallize as polypseudorotaxane precipitates.[24,29] The kinetic process can be monitored via time-dependent turbidity experiments.[35] For example, the transmittance of a γ-CD/PEG_{4k}-$(OH)_2$ mixture ([γ-CD] = 51.3 mM, [PEG_{4k}-$(OH)_2$] = 1.25 mM; Figure 2D) reached ≤20% in 920 min at 20°C. ^1H NMR analysis showed that an average of 21.7 γ-CDs were threaded on the PEG_{4k}-$(OH)_2$ in the crystalline precipitates (Figure 2E and Table S1). In comparison, the transmittance of the reaction of PEG_{4k}-$(nap)_2$ and γ-CD reached ≤1% only after 48 min, and 13.2 γ-CDs were threaded on PEG_{4k}-$(nap)_2$ in the polypseudorotaxanes (Figures 2D and 2E). When PEG_{4k}-$(azo)_2$ was used as the axle, the polypseudorotaxane formation and crystallization rates were further accelerated. The transmittance of the reaction of γ-CD (51.3 mM) and PEG_{4k}-$(azo)_2$ (1.25 mM) started to decrease after just 1 min and reached ≤1% in 17 min (Figure 2D). ^1H NMR analysis revealed that an average of 13.9 γ-CDs were threaded onto each PEG_{4k}-$(azo)_2$ axle (Figure 2E). Furthermore, unlike the sizable crystals of PEG_{4k}-$(OH)_2$/γ-CD polypseudorotaxanes observed under optical microscopy (Figure S18), micro-crystalline precipitates were formed by PEG_{4k}-$(azo)_2$ or PEG_{4k}-$(nap)_2$ and γ-CD. These results suggested that high-affinity-binding end groups of the PEG axle, such as the methacrylate azobenzene moieties, rapidly recruit γ-CDs in the solution to form stable 2:2 complexes. These stable complexes slow down the continuous γ-CD threading, resulting in an

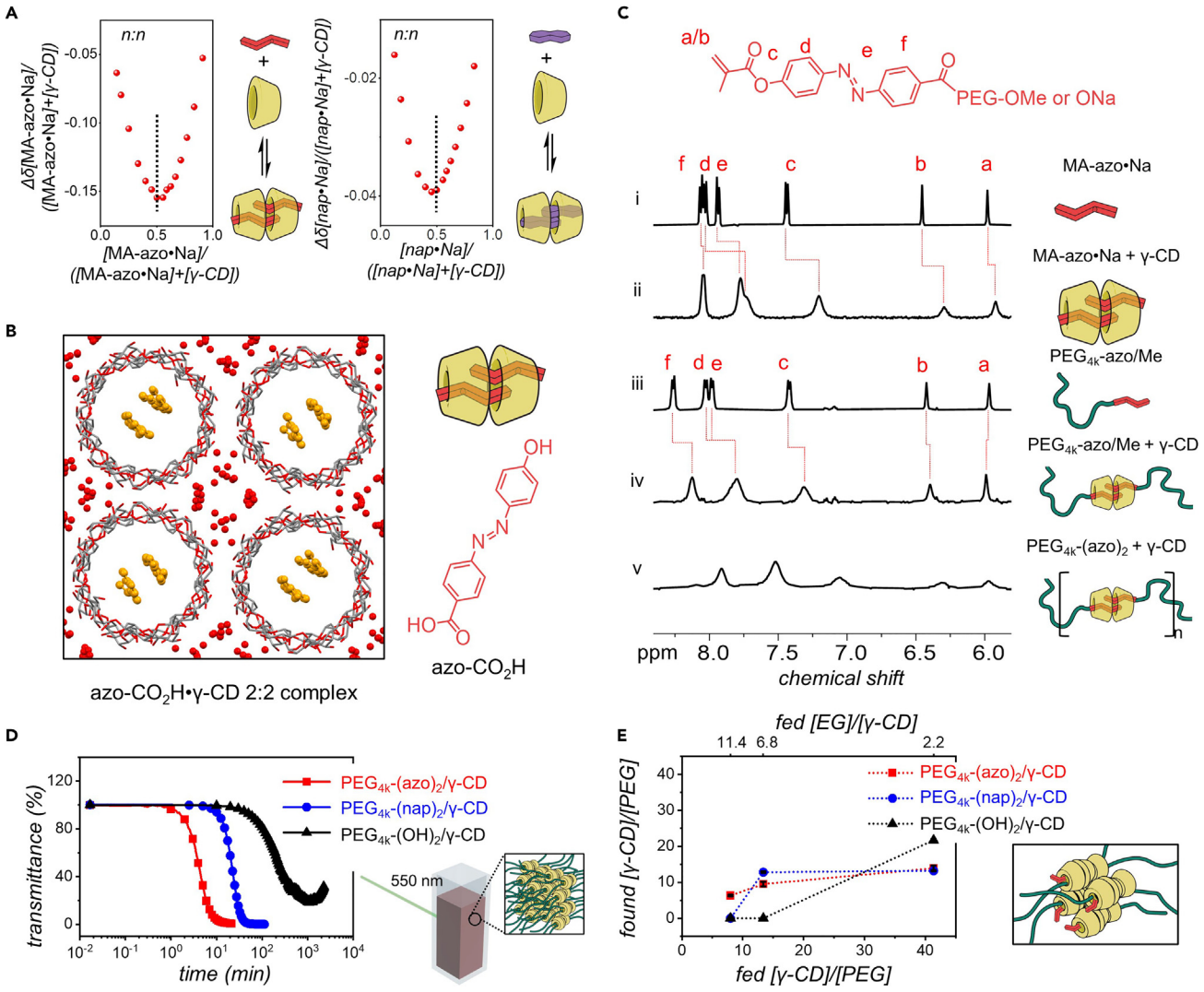

Figure 2. Synthesis and characterization of the pro-slide-ring crosslinker

(A) Job plots of MA-azo•Na and nap•Na with γ-CD in D_2O measured at 298 K.

(B) Single-crystal structure of an azo-CO_2H•γ-CD 2:2 complex.

(C) ^1H NMR spectra (500 MHz, 298 K, D_2O) of (i) 0.5 mM MA-azo•Na, (ii) 0.5 mM MA-azo•Na and 0.5 mM γ-CD, (iii) 0.5 mM PEG_{4k}-azo/Me, (iv) 0.5 mM PEG_{4k}-azo/Me and 0.5 mM γ-CD, and (v) 0.5 mM PEG_{4k}-$(azo)_2$ and 1.0 mM γ-CD.

(D) Time-dependent transmittances of the crystallization processes by mixing γ-CD with PEG_{4k}-$(azo)_2$, PEG_{4k}-nap_2, and PEG_{4k}-$(OH)_2$ at 20°C (optical path: 10 mm, λ = 550 nm). The concentrations of PEGs are 1.25 mM, and the concentration of γ-CD is 51.3 mM.

(E) The [γ-CD]/[PEG] threading number obtained from the ^1H NMR analysis of the precipitates at varied [γ-CD]/[PEG] fed ratios. For samples with no precipitation, the [γ-CD]/[PEG] ratio is set to 0.

early crystallization of polypseudorotaxanes with fewer threaded γ-CDs per PEG axle (Figure 1C).

The kinetically accelerated polypseudorotaxane formation and crystallization enabled us to trap fewer γ-CDs per PEG axle. When the feeding ratios of γ-CD to PEG were decreased from 41.4:1 to 13.4:1 and 8.0:1, no precipitation was observed during the reactions of γ-CD/PEG_{4k}-$(OH)_2$ (Figures 2E and S15). At a feed ratio of γ-CD:PEG_{4k}-$(nap)_2$ = 13.4:1, there were no transmittance changes until 400 min for the PEG_{4k}-$(nap)_2$/γ-CD polypseudorotaxane, which reached ≤80% after ~1,300 min with a γ-CD:PEG ratio of 11.5 (Figure S15). When the feeding

Please cite this article in press as: Tang et al., Reinforced double-threaded slide-ring networks for accelerated hydrogel discovery and 3D printing, Chem (2023), https://doi.org/10.1016/j.chempr.2023.07.020

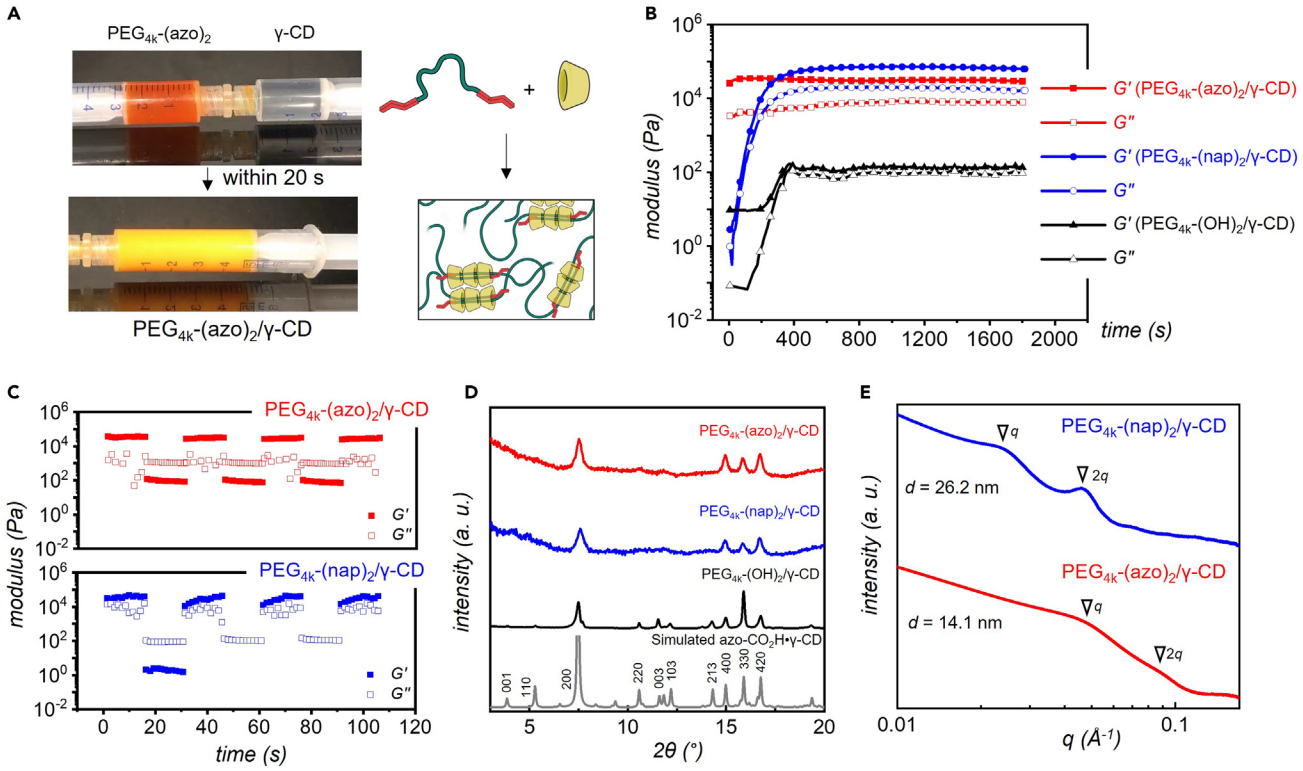

Figure 3. Formation and characterization of pro-slide-ring crosslinker hydrogels

(A) Images showing the rapid gelation upon mixing the aqueous solutions of PEG_{4k}-$(azo)_2$ and γ-CD.

(B) Time-dependent rheological measurements upon mixing solutions of PEG_{4k}-$(azo)_2$, PEG_{4k}-nap_2, and PEG_{4k}-$(OH)_2$ and γ-CD. Angular frequency: 10 rad/s. [PEG] = 15 mM, [γ-CD] = 120 mM.

(C) Step-strain profiles of polypseudorotaxane hydrogels composed of PEG_{4k}-$(azo)_2$/γ-CD (top) and PEG_{4k}-$(nap)_2$/γ-CD (bottom).

(D and E) WAXS (D) and SAXS (E) profiles of polypseudorotaxanes composed of PEG_{4k}-$(azo)_2$/γ-CD, PEG_{4k}-$(nap)_2$/γ-CD, and PEG_{4k}-$(OH)_2$/γ-CD. A simulated WAXS of the HO-azo_2•γ-CD_2 single crystal was used as a reference.

γ-CD:PEG_{4k}-$(nap)_2$ ratio was decreased to 8.0:1, no precipitation was observed (Figure S15). In sharp contrast, PEG_{4k}-$(azo)_2$/γ-CD polypseudorotaxanes rapidly formed and precipitated at the 41.4:1, 13.4:1, and 8.0:1 feeding ratios, and the time required for reaching 1% transmittance was 17, 29, and 88 min, respectively (Figure S15). The kinetically trapped γ-CDs per PEG_{4k}-$(azo)_2$ formed in three polypseudorotaxane precipitates were measured as 13.9, 7.2, and 5.8 (Figure 2E). These results suggested that the end groups of PEG_{4k}-$(azo)_2$ effectively stabilized the threaded γ-CDs to trigger early crystallization. This method offers a unique way to synthesize polypseudorotaxanes with fewer threaded γ-CDs, enabling the construction of slide-ring gels with larger ring-sliding distances.

Interestingly, viscoelastic polypseudorotaxane hydrogels were formed rapidly when γ-CD and PEG_{4k}-$(azo)_2$ were mixed at a higher concentration. As shown in Figure 3A, two syringes loaded with a γ-CD solution (120 mM) and a PEG_{4k}-$(azo)_2$ solution (15 mM) were connected via a Luer lock connector. Within just 20 s of back-and-forth mixing, an opaque viscoelastic hydrogel was formed at room temperature (Video S1)! Time-dependent angular frequency measurements showed that a stable hydrogel with elastic moduli $G' \approx 30$ kPa had already formed when the mixture was loaded onto the rheometer (Figure 3B). In comparison, the rate of gelation for PEG_{4k}-$(nap)_2$/γ-CD polypseudorotaxane reached a steady state after 5 min with $G' \approx 70$ kPa

Please cite this article in press as: Tang et al., Reinforced double-threaded slide-ring networks for accelerated hydrogel discovery and 3D printing, Chem (2023), https://doi.org/10.1016/j.chempr.2023.07.020

(Figure 3B). When PEG_{4k}-$(OH)_2$ (15 mM) was mixed with γ-CD (120 mM), white suspensions were formed after 5 min and exhibited elastic moduli of ~150 Pa and loss moduli G'' of ~100 Pa. Both PEG_{4k}-$(azo)_2$/γ-CD and PEG_{4k}-$(nap)_2$/γ-CD polypseudorotaxane hydrogels showed full recovery in the step-strain rheological sweeps (Figure 3C), whereas the PEG_{4k}-$(OH)_2$/γ-CD polypseudorotaxane suspension appeared as a Newtonian liquid upon shearing (Figure S26). The outstanding viscoelastic properties of PEG_{4k}-$(azo)_2$/γ-CD and PEG_{4k}-$(nap)_2$/γ-CD hydrogels are attributed to the formation of micro-crystalline domains similar to those of 3D-printable α-CD-based polypseudorotaxane hydrogels.[20,35,36] To probe the super-structures in these hydrogels, we collected wide- and small-angle X-ray scattering (WAXS and SAXS) diffraction profiles of the samples and used the simulated diffraction profile of the $(azo\text{-}CO_2H)_2$•$(\gamma\text{-CD})_2$ single crystal as a reference. The WAXS profiles of the PEG_{4k}-$(OH)_2$/γ-CD, PEG_{4k}-$(nap)_2$/γ-CD, and PEG_{4k}-$(azo)_2$/γ-CD polypseudorotaxane samples matched the diffraction profiles of $(azo\text{-}CO_2H)_2$•$(\gamma\text{-CD})_2$ (Figure 3E), confirming the presence of γ-CD-based crystalline domains. The WAXS profile of PEG_{4k}-$(OH)_2$/γ-CD was significantly sharper than those of the PEG_{4k}-$(nap)_2$/γ-CD and PEG_{4k}-$(azo)_2$/γ-CD polypseudorotaxane hydrogels, suggesting that the sizes of the crystalline domains in these hydrogels are smaller according to the Scherrer equation.[37] In SAXS analysis (Figure 3F), the PEG_{4k}-$(azo)_2$/γ-CD hydrogel showed diffractions fitted to lamellar structures with d-spacing distances of 14.1 nm, indicating that the crystalline domains consist of ~18.5 γ-CDs. A larger d = 26.2 nm was fitted to the PEG_{4k}-$(nap)_2$/γ-CD hydrogel, corresponding to crystalline domains of 34.4 γ-CDs. These results suggest that smaller and less-defined crystalline domains than those in the PEG_{4k}-$(nap)_2$/γ-CD hydrogel were formed in the PEG_{4k}-$(azo)_2$/γ-CD hydrogel.

When the methacrylate groups of PEG_{4k}-$(azo)_2$/γ-CD polypseudorotaxanes are copolymerized with commodity co-monomers, the pro-slide-ring crosslinkers are converted to crystalline-domain-reinforced slide-ring (CrysDoS)-gels (Figure 4A). These CrysDoS-gels possess unique network features, including crystalline-domain crosslinkages and dormant slide-ring joints that can be activated upon the disruption of the crystalline domains. To synthesize a CrysDoS hydrogel (see supplemental experimental procedures section S6 for details), we utilized a pro-slide-ring crosslinker consisting of PEG and γ-CD, along with a co-monomer, and initiators tetramethylethylenediamine (TMEDA) and ammonium persulfate (APS). As a result, these hydrogels are designated as $CrysDoS_{(a,\ b)\text{-}X}$, where a and b represent the millimolar concentrations of PEG and γ-CD, respectively, and X denotes the specific type of co-monomer employed.

We synthesized a $CrysDoS_{(15,\ 120)\text{-}HEMA}$-gel by first combining the pro-slide-ring crosslinker with hydroxyl ethylene methacrylate (HEMA; Figure 4A) to form a precursor hydrogel, which then underwent covalent crosslinking (see supplemental experimental procedures section S6.1). The elastic modulus G' (22 kPa; Figure S31) of the precursor hydrogel was slightly smaller than that of the pro-slide-ring hydrogel (36 kPa; Figure S24) because the large excess of the HEMA co-monomer competed with the PEG axle for γ-CD binding. After crosslinking, the conversion of the methacrylate groups for PEG_{4k}-$(azo)_2$ was determined to be >90% through ^1H NMR swelling and digestion experiments (Table S5). For comparative purposes, a control hydrogel in the absence of γ-CD (Ctrl-gel; Figure 4) was also synthesized. We washed the $CrysDoS_{(15,\ 120)\text{-}HEMA}$-gel and Ctrl-gel extensively to remove unreacted species and immersed them in Na_2SO_4 aqueous solutions to reach the same water content of 46 wt %. WAXS analysis (Figure 4B) showed that the γ-CD crystalline domains were well preserved in the $CrysDoS_{(15,\ 120)\text{-}HEMA}$-gel. SAXS analysis showed a

Please cite this article in press as: Tang et al., Reinforced double-threaded slide-ring networks for accelerated hydrogel discovery and 3D printing, Chem (2023), https://doi.org/10.1016/j.chempr.2023.07.020

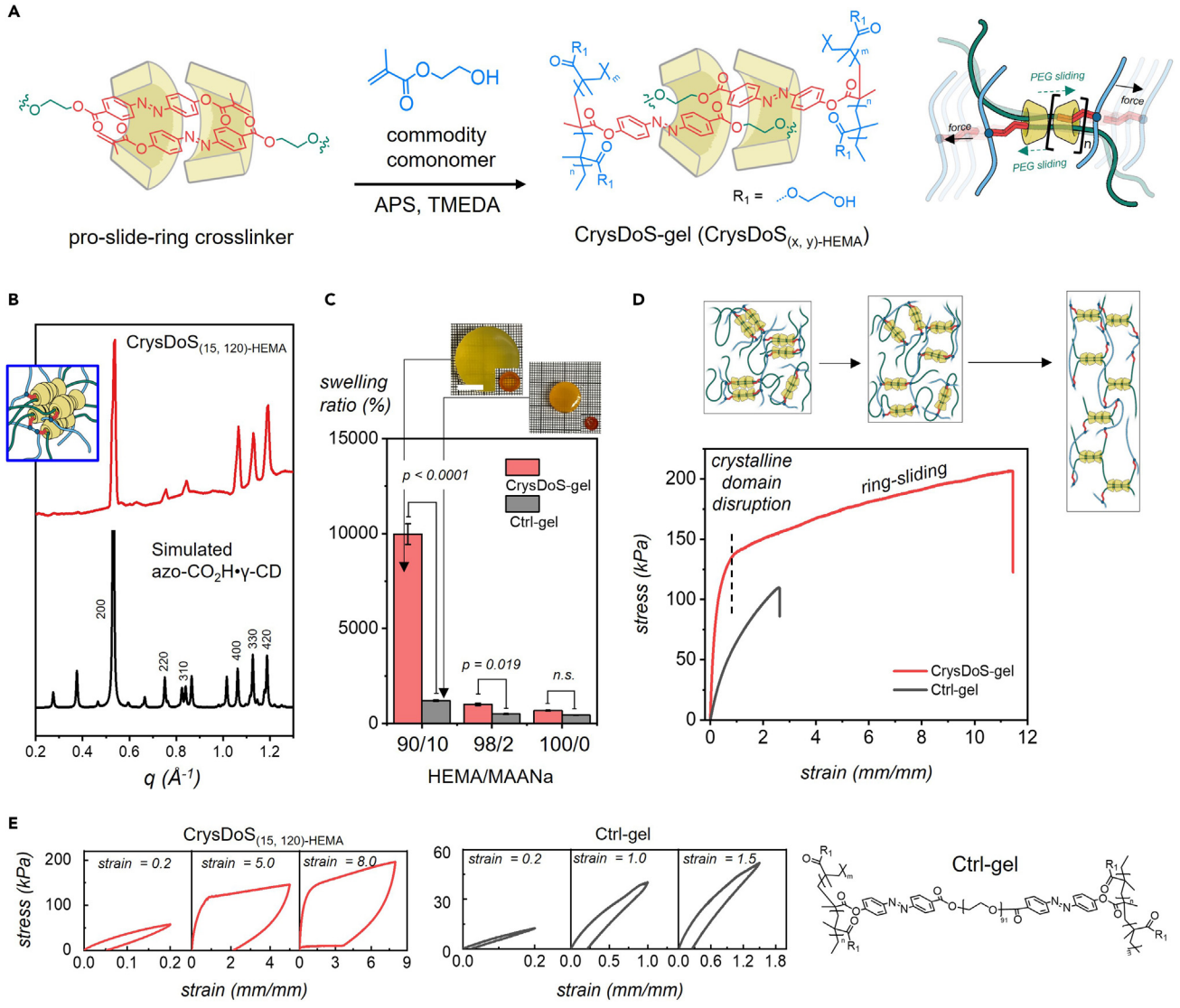

Figure 4. Synthesis and characterizations of CrysDoS-gels

(A) Synthetic scheme of CrysDoS$_{(15,\ 120)\text{-HEMA}}$-gel with the pro-slide-ring crosslinker and HEMA. The Ctrl-gel is shown in (E).

(B) WAXS profiles of the CrysDoS$_{(15,\ 120)\text{-HEMA}}$-gel and a (azo–$CO_2H)_2$•(γ-CD)$_2$ 2:2 complex single-crystal (simulated from X-ray structure).

(C) The swelling behaviors of CrysDoS-gels and Ctrl-gels with different amounts of MAANa co-monomer (10, 2, and 0 mol%, averaged value of five samples). Inset: images of these CrysDoS-gel and Ctrl-gels in their fully swelled and dried states (scale bars: 10.0 mm). The p values were calculated with a one-way analysis of variance (ANOVA) followed by post hoc Tukey multiple-comparison tests. n.s., not significant.

(D and E) Tensile stress-strain (D) and cyclic-loading (E) profiles of CrysDoS$_{(15,\ 120)\text{-HEMA}}$-gel and Ctrl-gel at room temperature (sizes: 30.0 × 8.0 × 2.0 mm, gauge length = 3.0 mm, strain rate = 1.5 mm/min).

lamellar structure with a *d*-spacing distance of 14.0 nm (Figure S37), similar to that of the pro-slide-ring gel, indicating that the addition of co-monomers had a minimal impact on the crystalline domains in the synthesized CrysDoS-gel.

When the crystalline domains of the CrysDoS$_{(15,\ 120)\text{-HEMA}}$-gel are disrupted, the hydrogel should undergo significant swelling as a result of the sliding motions of γ-CDs, similarly to traditional slide-ring gels.[14,23,29,30] However, the swelling ratio of the CrysDoS$_{(15,\ 120)\text{-HEMA}}$-gel was measured as 690% ± 20% (Figure 4C), which is comparable to that of the Ctrl-gel, indicating that the crystalline domains of the

Please cite this article in press as: Tang et al., Reinforced double-threaded slide-ring networks for accelerated hydrogel discovery and 3D printing, Chem (2023), https://doi.org/10.1016/j.chempr.2023.07.020

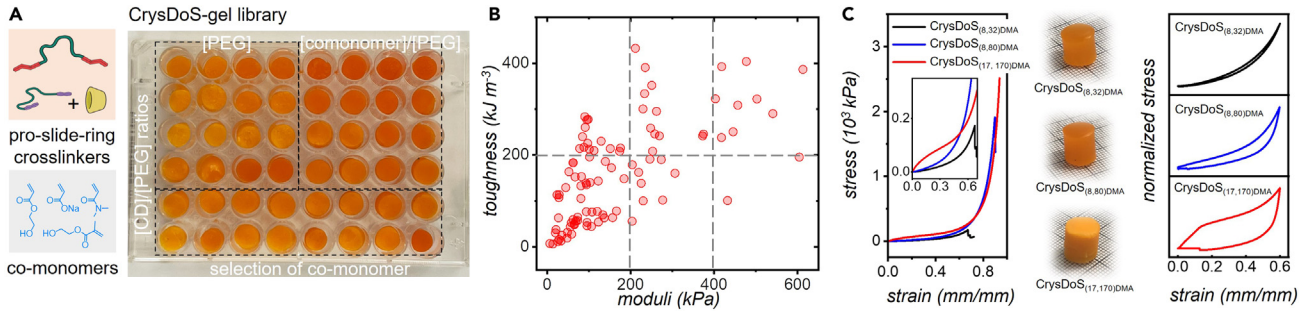

Figure 5. High-throughput CrysDoS-gel synthesis and mechanical characterizations

(A) High-throughput synthesis of CrysDoS-gels in a 48-well plate and their various chemical inputs.

(B) The measured toughness versus compressive moduli of the CrysDoS-gel library.

(C) Compressive stress-strain and cyclic-loading profiles of CrysDoS$_{(8,\ 32)\text{-DMA}}$ (black), CrysDoS$_{(8,\ 80)\text{-DMA}}$ (blue), and CrysDoS$_{(17,\ 170)\text{-DMA}}$ (red).

CrysDoS-gel remained largely intact. Adding small amounts of the ionic co-monomer sodium methacrylate (MAANa) gradually increased the osmotic pressure for swelling, disrupting the crystalline domains in the CrysDoS-gel. At an MAANa/HEMA ratio of 1:9, the CrysDoS$_{(15,\ 120)\text{-HEMA/MAANa}}$-gel demonstrated a significantly higher swelling ratio of 10,000% $\pm$ 500%, nearly ten times larger than that of the Ctrl$_{\text{HEMA/MAANa}}$-gel (Figure 4C) as a result of the activated mobile γ-CD joints.

The CrysDoS$_{(15,\ 120)\text{-HEMA}}$-gel exhibited a high Young's modulus (E = 520 $\pm$ 20 kPa) and high stretchability (11.4 $\pm$ 1.3 mm/mm) in the uniaxial tensile tests (Figure 4D; see supplemental experimental procedures section S6.3 for detailed information), whereas the Ctrl-gel showed E = 100 $\pm$ 10 kPa and 2.6 $\pm$ 0.4 mm/mm stretchability. Considering that traditional slide-ring gels usually have similar Young's moduli to their fixed crosslinked counterparts,[21] the 5-fold higher Young's modulus here highlights the benefits of the γ-CD crystalline-domain reinforcements. Notably, the tensile profile of the CrysDoS$_{(15,\ 120)\text{-HEMA}}$-gel exhibited a two-stage characteristic. At low strains ($\leq$0.5 mm/mm), the CryDoS-gel underwent an elastic deformation whereby the tensile stress reached ~130 kPa as a result of the disruption of the crystalline domain. At higher strains, the released mobile γ-CDs slid upon stretching, and the tensile stress gradually increased to ~200 kPa (Figure 4D), similarly to that of traditional slide-ring gels.[20,23,38,39] The high Young's modulus and high stretchability of the CrysDoS$_{(15,\ 120)\text{-HEMA}}$-gel resulted in a high toughness of 2.1 $\pm$ 0.3 MJ/m^3, 10-fold higher than that of the Ctrl-gel (0.19 $\pm$ 0.05 MJ/m^3; Table S6). In the cyclic loading-unloading tensile measurements (Figure 4E), the CrysDoS$_{(15,\ 120)\text{-HEMA}}$-gel showed a large hysteresis ($1 - U_2/U_1$) of 0.77 and 0.74 at strains of 5.0 and 8.0 mm/mm, respectively, larger than those of the Ctrl-gel (Figure 4E). These results highlight the benefits of the design of CrysDoS-gels for enhanced mechanical performance.

We leveraged the rapid gelation of the pro-slide-ring crosslinkers and modular synthesis of CrysDoS-gel to create a library of materials by varying the compositions of the pro-slide-ring crosslinkers and introducing different water-soluble co-monomers, such as dimethylacrylamide (DMA), hydroxyl ethylene acrylate with sodium acrylate (HEA/AANa), and HEMA (Figure 5A). Hence, we performed a high-throughput CrysDoS-gel synthesis (Figure 5A) with varied PEG$_{4k}$-(azo)$_2$ concentrations (8–17 mM), [γ-CD]/[PEG$_{4k}$-(azo)$_2$] ratios (0–14), co-monomers, and [co-monomer]/[PEG$_{4k}$-(azo)$_2$] ratios (100 and 150). Additionally, we used a non-reactive PEG$_{4k}$-(nap)$_2$ axle as a competing axle agent, which will only contribute to the

Please cite this article in press as: Tang et al., Reinforced double-threaded slide-ring networks for accelerated hydrogel discovery and 3D printing, Chem (2023), https://doi.org/10.1016/j.chempr.2023.07.020

formation of crystalline domains in the hydrogel and will not form slide-ring joints. Stock solutions of the pro-slide-ring crosslinker components and co-monomers were mixed in multiple 48-well plates for gelation, followed by polymerization, generating a library of 96 CrysDoS-gels (Figure 5B; for a detailed synthetic method, see supplemental experimental procedures section S7.1). Notably, the gelation time of these samples remained short (<1 min), where slight variations depended on the co-monomer selection and precursor concentrations (see supplemental experimental procedures section S6.1).

To investigate the mechanical properties of these CrysDoS-gels in a time- and cost-effective manner, we performed uniaxial compressive and cyclic (un)loading tests. These analyses yielded a comprehensive dataset encompassing experimental measurements of compressive moduli (E), compressive toughness (U), and mechanical hysteresis ($1 - U_2/U_1$) for all 96 CrysDoS-gels (supplemental experimental procedures section S7). The library of CrysDoS-gels exhibited a broad range of mechanical features such that compressive moduli and toughness spanned two orders of magnitude (E = 7.2–600 kPa, U = 6.0–500 kJ/m^3; Figure 5B). The synthesized CrysDoS-gels were classified into three categories: soft and brittle, soft and tough, and rigid and tough. To illustrate each category, we selected three representative CrysDoS-gels for further discussion (Figure 5C).

In the soft and brittle category, exemplified by the CrysDoS$_{(8,\ 32)\text{-DMA}}$-gel synthesized at a low [γ-CD]/[PEG] ratio, the gel displayed a compressive modulus of E = 59 kPa and a strain at break of σ_{break} = 67% (Figure 5D, black). This gel exhibited the typical behavior of a covalently crosslinked network with minimal hysteresis observed in the cyclic (un)loading test (Figure 5C, black). In the soft and tough category, when the [γ-CD]/[PEG] ratio was increased to 10, the CrysDoS$_{(8,\ 80)\text{-DMA}}$-gel showed an enhanced compressibility of σ_{break} = 91% while maintaining a similar compressive modulus of E = 101 kPa (Figure 5C, blue). The third category was represented by the CrysDoS$_{(17,\ 170)\text{-DMA}}$-gel, which possessed a higher concentration of pro-slide-ring crosslinkers, resulting in a rigid and tough gel. The CrysDoS$_{(17,\ 170)\text{-DMA}}$-gel showed both a high compressive modulus of E = 541 kPa and a high compressibility of σ_{break} > 94% (Figure 5C, red). Furthermore, the CrysDoS$_{(8,\ 80)\text{-DMA}}$ and CrysDoS$_{(17,\ 170)\text{-DMA}}$ hydrogels exhibited notable hysteresis of ($1 - U_2/U_1$) = 0.61 and 0.79, respectively (Figure 5C, blue and red), suggesting that the hydrogen bonding between neighboring γ-CDs was disrupted upon compression to activate slide-ring motions. The remarkable combination of high compressive modulus and high toughness in the CrysDoS$_{(17,\ 170)}$-gel showcases the successful design of a crystalline-domain-reinforced double-threaded slide-ring network, breaking the traditional trade-off between elasticity and toughness in slide-ring gels.

The high-throughput synthesis of CrysDoS-gels opened up a large material design space; however, it also introduced a complex structure-property relationship for interpretation. Hence, we employed data science tools such as random forest (machine learning)[40–44] and multivariate linear regression analysis[45,46] to ascertain connections between the chemical composition of CrysDoS-gels and their material properties (Figure 6). The chemical variables used for modeling the dataset of 96 CrysDoS-gels consisted of PEG concentration, [γ-CD]/[PEG], types of monomers, [co-monomer]/[PEG], and [PEG$_{4k}$-(nap)$_2$]/[PEG]. Separate models were created for each of the associated mechanical properties of the hydrogels, such as compressive moduli, compressive toughness, and hysteresis. We partitioned the dataset into a training set (70% of the data) for training each model and a test set (30%) for validating

Please cite this article in press as: Tang et al., Reinforced double-threaded slide-ring networks for accelerated hydrogel discovery and 3D printing, Chem (2023), https://doi.org/10.1016/j.chempr.2023.07.020

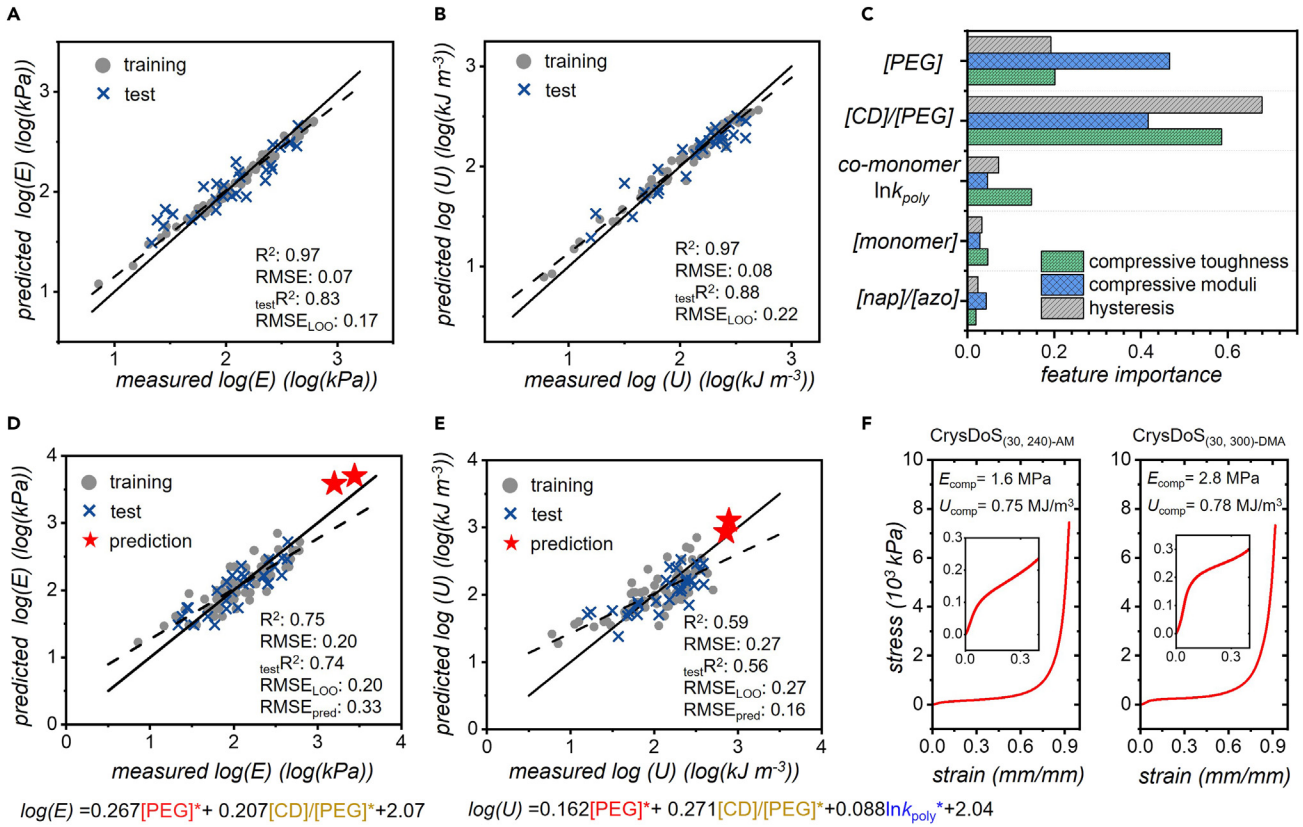

Figure 6. Implementation of data science for the prediction of material properties and the discovery of CrysDoS-gels

(A and B) Machine-learning models using random forest regression, where a 70:30 train-test partition (using kernel density estimation) was employed for the prediction of (A) compressive moduli and (B) compressive toughness for 96 CrysDoS-gels. The solid black line is the y = x line, and the dashed black line is the line of best fit.

(C) A bar plot depicting the importance of all five input features used for training the random forest models predicting hysteresis, compressive moduli, and compressive toughness of CrysDoS-gels.

(D and E) Multivariate linear regression models for the prediction of (D) compressive moduli and (E) compressive toughness of CrysDoS-gels. These models were used for predicting better-performing CrysDoS-gels. The solid black line is the y = x line, and the dashed black line is the line of best fit.

(F) Uniaxial compressive profiles of $CrysDoS_{(30,\ 240)\text{-AM}}$ and $CrysDoS_{(30,\ 300)\text{-DMA}}$. Strain rate: 1 mm/min.

the predictive power of each model. We held back 30% of the data during the model development in addition to conducting other cross-validation techniques, such as leave one out (LOO) and *k*-fold (where $k = 5$), to prevent overfitting and ensure that the models were not heavily biased toward specific data points over others.

We utilized a machine-learning algorithm, random forest, to develop models for compressive moduli (Figure 6A), toughness (Figure 6B), and hysteresis (Figures S73 and S74) of the CrysDoS-gels. We optimized these models by using feature selection and hyperparameter optimization.[40] We evaluated the performance of the models by using the test set, which demonstrated a good fit with high R^2 values and the absence of significant outliers. Random forest analysis provided insights into the importance of different chemical features in relation to the mechanical properties (Figure 6C). The composition of the pro-slide-ring crosslinker, which includes the PEG concentration and the ratio of [γ-CD]/[PEG], emerged prominently as the most influential feature affecting the compressive moduli, toughness, and hysteresis of the synthesized CrysDoS-gels. By contrast, the rate of polymerization affected the toughness more significantly than compressive moduli or

Please cite this article in press as: Tang et al., Reinforced double-threaded slide-ring networks for accelerated hydrogel discovery and 3D printing, Chem (2023), https://doi.org/10.1016/j.chempr.2023.07.020

hysteresis.[47] Intriguingly, the addition of the competing PEG_{4k}-$(nap)_2$ axle or the types of co-monomer had negligible contributions to the mechanical properties of the CrysDoS-gels.

Although the random forest analysis highlighted the pro-slide-ring crosslinker as the primary contributor to the mechanical properties of the CrysDoS-gels, this algorithm was unable to predict data outside of the range it was trained on. Hence, we performed multivariate linear regression analysis to obtain a quantitative relationship between the chemical features and mechanical properties, which allowed us to extrapolate beyond the range of the dataset and predict superior Crys-DoS-gels (Figures 6D and 6E). Although these models are not as statistically powerful as the models obtained with random forest, the same key features representing pro-slide-ring crosslinkers and polymerization rates ([PEG], [γ-CD]/[PEG], and lnk_{poly}) were identified as main contributors to the material properties of the CrysDoS-gels. To validate the predictive power of these models, we synthesized two gels, $CrysDoS_{(30,\ 300)\text{-}DMA}$ and $CrysDoS_{(30,\ 240)\text{-}AM}$ (AM = acrylamide), with an increased amount of pro-slide-ring crosslinker and faster-reacting co-monomers. The compressive moduli of $CrysDoS_{(30,\ 300)\text{-}DMA}$ and $CrysDoS_{(30,\ 240)\text{-}AM}$ were measured as 2.8 and 1.6 MPa, respectively (Figure 6F), and their toughness was measured as 0.78 and 0.75 MJ/m^3, respectively (Figure 6F). Both the compressive moduli and toughness of these two CrysDoS-gels outperformed those of the best hydrogels synthesized in the high-throughput experiments (E_{max} = 0.6 MPa, U_{max} = 0.5 MJ/m^3). Not only do these discoveries verify the predictive power of the multivariate linear regression models, but more importantly, they demonstrate the feasibility of exploring stronger CrysDoS-gels by using data science to understand the structure-property relationship.

The broad range of mechanical properties of the CrysDoS-gel library and their similar chemical compositions make them ideal for constructing stress-sensing devices with combined high sensitivity and large force detection range via DIW 3D printing. The rapid gelation and excellent rheological features of the pro-slide-ring crosslinker PEG_{4k}-$(azo)_2$/γ-CD hydrogels make them ideal for DIW. The PEG_{4k}-$(azo)_2$/γ-CD polypseudorotaxane hydrogels in the presence of co-monomers were printed into woodpile lattice cubes with good structural integrity (Figure 7A). They were converted to lattices of $CrysDoS_{(15,\ 120)\text{-}HEA/AANa}$ after copolymerization with good compressibility and rapid shape recovery.

To design a high-performance capacitive stress sensor, we specifically selected $CrysDoS_{(8,\ 48)\text{-}HEA/AANa}$ and $CrysDoS_{(17,\ 136)\text{-}HEA/AANa}$, which have drastically different compressive moduli (24 and 263 kPa, respectively), from the library (Figure 7B). These molded CrysDoS-gels showed a single linear response in terms of the relative capacitance change ($\Delta C/C_0$) with respect to the applied stress. $CrysDoS_{(8,\ 48)\text{-}HEA/AANa}$ exhibited a higher stress sensitivity (50 ± 9 MPa^{-1}) but a lower range of detection (0–30 kPa). $CrysDoS_{(17,\ 136)\text{-}HEA/AANa}$ showed a higher range of detection (0–150 kPa) but a reduced sensitivity (13 ± 4 MPa^{-1}) (Figure 7C). Although the rheological properties of the pro-slide-ring crosslinker for $CrysDoS_{(8,\ 48)\text{-}HEA/AANa}$-gel only allowed for extrusion, $CrysDoS_{(17,\ 136)\text{-}HEA/AANa}$-gel was successfully 3D printed as a self-supporting cube (9.0 × 9.0 × 10.8 mm). This cube showed a two-stage linear relationship and significantly improved sensitivity at a lower pressure range (<10 kPa; Figure 7C, black dot). The sensitivity of the first stage was measured to be 130 ± 15 MPa^{-1} (Figure 7D), and the second stage was measured to be 30 ± 10 MPa^{-1}. We believe the structural anisotropy and small voids introduced during the 3D-printing process enhanced its sensitivity without compromising its range of detection (Figure 7D).

Please cite this article in press as: Tang et al., Reinforced double-threaded slide-ring networks for accelerated hydrogel discovery and 3D printing, Chem (2023), https://doi.org/10.1016/j.chempr.2023.07.020

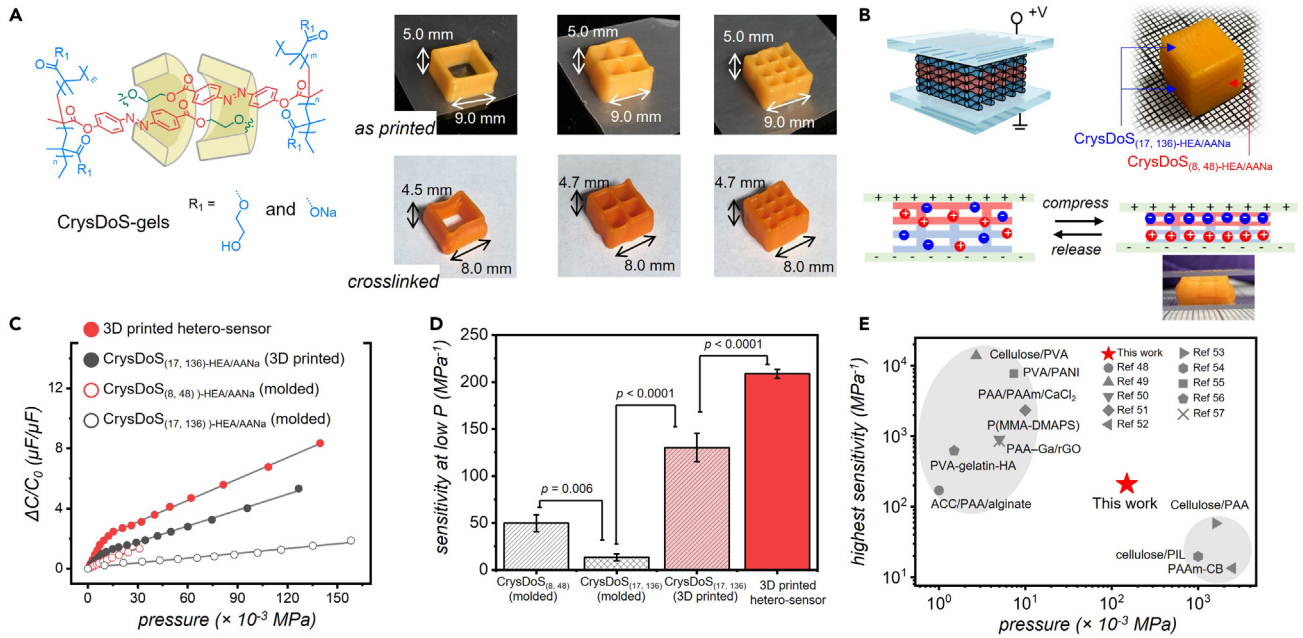

Figure 7. 3D printing of ionic CrysDoS-gels as stress sensors

(A) 3D-printed CrysDoS$_{(15,\ 120)\text{-HEA/AANa}}$ lattices using the pro-slide-ring hydrogel inks.

(B) 3D-printed heterogeneous capacitive stress sensor using CrysDoS$_{(17,\ 136)\text{-HEA/AANa}}$ and CrysDoS$_{(8,\ 48)\text{-HEA/AANa}}$ inks.

(C) Plots of relative capacitance changes of molded CrysDoS$_{(8,\ 48)\text{-HEA/AANa}}$, molded CrysDoS$_{(17,\ 136)\text{-HEA/AANa}}$, 3D-printed CrysDoS$_{(17,\ 136)\text{-HEA/AANa}}$, and 3D-printed hetero-sensor upon compression.

(D) Comparison of the low-pressure stress sensitivity (0–10 kPa) of the molded CrysDoS$_{(8,\ 48)\text{-HEA/AANa}}$, molded CrysDoS$_{(17,\ 136)\text{-HEA/AANa}}$, 3D-printed CrysDoS$_{(17,\ 136)\text{-HEA/AANa}}$, and 3D-printed heterosensor samples. The p values were calculated with a one-way ANOVA followed by post hoc Tukey multiple-comparison tests of three samples.

(E) A performance plot comparing the sensitivity and the range of detection of this work with state-of-the-art hydrogel-based capacitive stress sensors.[48–57]

When we constructed a heterogeneous 3D-printed cube (9.0 × 9.0 × 10.8 mm) by using the extrudable CrysDoS$_{(8,\ 48)\text{-HEA/AANa}}$ and 3D-printable CrysDoS$_{(17,\ 136)\text{-HEA/AANa}}$ (see the supplemental information for details), the sandwich-structured sensor showed a similar two-stage linear relationship (Figure 7C, red dot) and exhibited further enhanced stress sensitivity of 209 $\pm$ 5 MPa^{-1} at the first stage (Figure 7D) and a sensitivity of 37 $\pm$ 9 MPa^{-1}, comparable to that of 3D-printed CrysDoS$_{(17,\ 136)\text{-HEA/AANa}}$, at the second stage. The combined high sensitivity and range of detection of this heterogeneous stress sensor outperform those of other state-of-the-art hydrogel materials[48–57] (Figure 7E). Clearly, the integration of compositionally similar but mechanically distinctive CrysDoS-gels through 3D printing overcomes the trade-off between sensitivity and range of detection in traditional stress-sensor designs, which will enable their potential applications for monitoring physiological signals, detecting environmental changes, or controlling robotic devices.

DISCUSSION

In summary, we have introduced a new strategy for overcoming the elasticity-toughness trade-off in traditional slide-ring network design by introducing crystalline-domain-reinforced double-threaded slide-ring networks. The key building block in this design is the pro-slide-ring crosslinker, formed through the self-assembly of γ-CDs and telechelic PEGs. We discovered that the rapid self-assembly between the acrylate-azobenzenyl end groups of the PEG not only facilitates rapid gelation but also controls the number of threaded γ-CDs on the PEG through kinetic

Please cite this article in press as: Tang et al., Reinforced double-threaded slide-ring networks for accelerated hydrogel discovery and 3D printing, Chem (2023), https://doi.org/10.1016/j.chempr.2023.07.020

crystallization. These pro-slide-ring crosslinkers exhibit desirable viscoelastic properties for DIW 3D printing because of the presence of micro-crystalline γ-CD/end-group domains.

By copolymerizing the modular pro-slide-ring crosslinkers with water-soluble comonomers, we synthesized 3D-printable crystalline-domain-reinforced slide-ring hydrogels with high elastic moduli and toughness, surpassing the limitations in traditional slide-ring gels. Furthermore, the modular synthesis enabled a high-throughput discovery of double-threaded slide-ring hydrogels, leading to the construction of a library of 96 hydrogels with diverse mechanical properties. Leveraging data science tools such as random forest and multivariate linear regression analysis, we have established a clear structure-property relationship by identifying the composition of the pro-slide-ring crosslinker as the key determinant of compressive moduli, compressive toughness, and hysteresis in the hydrogels. We discovered two new slide-ring hydrogels with superior mechanical performance predicted by the linear regression model. Moreover, we selected two hydrogels from this library and fabricated a heterogeneous capacitive stress sensor by using DIW 3D printing. This sensor demonstrated high stress sensitivity and a broad detection range, outperforming the capabilities of most state-of-the-art hydrogel sensors.

Overall, our new synthetic approach for constructing robust slide-ring networks—combined with modular high-throughput synthesis, data-science-aided establishment of structure-property relationships, and stress-sensor fabrication—demonstrates the power of designing mechanically robust networks through molecular design. This approach holds great potential for accelerating the discovery of rigid and tough slide-ring networks.

EXPERIMENTAL PROCEDURES

Resource availability

Lead contact

Requests for further information and resources should be directed to and will be fulfilled by the lead contact, Chenfeng Ke (chenfeng.ke@dartmouth.edu).

Materials availability

All unique reagents generated in this study are available from the lead contact without restriction.

Data and code availability

The X-ray datasets generated during this study are available at the Cambridge Crystallographic Data Centre (CCDC) (https://www.ccdc.cam.ac.uk) under deposition numbers CCDC: 2175910 and 2192621. The scripts used for data science analysis and the 3D printing scripts generated in this study are available from the lead contact.

SUPPLEMENTAL INFORMATION

Supplemental information can be found online at https://doi.org/10.1016/j.chempr.2023.07.020.

ACKNOWLEDGMENTS

This work was supported by the Basic Energy Sciences program of the US Department of Energy (DOE) (DE-SC0022267), the Beckman Young Investigator program

of the Arnold and Mabel Beckman Foundation, and the Dartmouth College Neukom Institute for Computational Science. C.K. appreciates the support of the Cottrell Scholar program of the Research Corporation for Science Advancement. D.Z. is supported by the National Science Foundation (EPSCoR-1757371). J.S. is supported by the Beckman Young Investigator program. This research used beamline 11BM (CMS) of the National Synchrotron Light Source II and the Center of Functional Nanomaterials (CFN), both of which are US DOE Office of Science User Facilities operated by the DOE Office of Science by Brookhaven National Laboratory under contract no. DE-SC0012704. We thank Dr. Errui Li for helping with the crystallization of the inclusion complex.

AUTHOR CONTRIBUTIONS

M.T. and C.K. conceived the design of this work and jointly drafted the manuscript with the assistance of J.A.R. M.T. performed most of the research. D.Z. synthesized PEG-$(nap)_2$, and J.S. refined the SCXRD structure. E.H.R.T. performed the SAXS analysis. H.Q. supported the initial research explorations in his lab during the COVID-19 pandemic. M.T. performed the data science analysis with the guidance of J.A.R.

DECLARATION OF INTERESTS

C.K. and M.T. have filed a provisional patent application: US 63/530,354.

Received: May 25, 2023
Revised: June 30, 2023
Accepted: July 31, 2023
Published: August 23, 2023

REFERENCES

1. Daly, A.C., Riley, L., Segura, T., and Burdick, J.A. (2020). Hydrogel microparticles for biomedical applications. Nat. Rev. Mater. *5*, 20–43. https://doi.org/10.1038/s41578-019-0148-6.

2. Peppas, N.A., Bures, P., Leobandung, W., and Ichikawa, H. (2000). Hydrogels in pharmaceutical formulations. Eur. J. Pharm. Biopharm. *50*, 27–46. https://doi.org/10.1016/S0939-6411(00)00090-4.

3. Li, J., and Mooney, D.J. (2016). Designing hydrogels for controlled drug delivery. Nat. Rev. Mater. *1*, 1–17. https://doi.org/10.1038/natrevmats.2016.71.

4. Zhao, X., Chen, X., Yuk, H., Lin, S., Liu, X., and Parada, G. (2021). Soft materials by design: unconventional polymer networks give extreme properties. Chem. Rev. *121*, 4309–4372. https://doi.org/10.1021/acs.chemrev.0c01088.

5. Yang, C., and Suo, Z. (2018). Hydrogel ionotronics. Nat. Rev. Mater. *3*, 125–142. https://doi.org/10.1038/s41578-018-0018-7.

6. Zhang, Y.S., and Khademhosseini, A. (2017). Advances in engineering hydrogels. Science *356*, eaaf3627. https://doi.org/10.1126/science.aaf3627.

7. Nicolson, P.C., and Vogt, J. (2001). Soft contact lens polymers: an evolution. Biomaterials *22*, 3273–3283. https://doi.org/10.1016/S0142-9612(01)00165-X.

8. Gilchrist, T., and Martin, A.M. (1983). Wound treatment with Sorbsan—an alginate fibre dressing. Biomaterials *4*, 317–320. https://doi.org/10.1016/0142-9612(83)90036-4.

9. Gu, Y., Zhao, J., and Johnson, J.A. (2020). Polymer networks: from plastics and gels to porous frameworks. Angew. Chem. Int. Ed. *59*, 5022–5049. https://doi.org/10.1002/anie.201902900.

10. Danielsen, S.P.O., Beech, H.K., Wang, S., El-Zaatari, B.M., Wang, X., Sapir, L., Ouchi, T., Wang, Z., Johnson, P.N., Hu, Y., et al. (2021). Molecular characterization of polymer networks. Chem. Rev. *121*, 5042–5092. https://doi.org/10.1021/acs.chemrev.0c01304.

11. Gong, J.P., Katsuyama, Y., Kurokawa, T., and Osada, Y. (2003). Double-network hydrogels with extremely high mechanical strength. Adv. Mater. *15*, 1155–1158. https://doi.org/10.1002/adma.200304907.

12. Nonoyama, T., and Gong, J.P. (2021). Tough double network hydrogel and its biomedical applications. Annu. Rev. Chem. Biomol. Eng. *12*, 393–410. https://doi.org/10.1146/annurev-chembioeng-101220-080338.

13. Sun, J.Y., Zhao, X., Illeperuma, W.R.K., Chaudhuri, O., Oh, K.H., Mooney, D.J., Vlassak, J.J., and Suo, Z. (2012). Highly stretchable and tough hydrogels. Nature *489*, 133–136. https://doi.org/10.1038/nature11409.

14. Okumura, Y., and Ito, K. (2001). The polyrotaxane gel: a topological gel by figure-of-eight cross-links. Adv. Mater. *13*, 485–487. https://doi.org/10.1002/1521-4095(200104)13:7<485::AID-ADMA485>3.0.CO;2-T.

15. Liu, C., Morimoto, N., Jiang, L., Kawahara, S., Noritomi, T., Yokoyama, H., Mayumi, K., and Ito, K. (2021). Tough hydrogels with rapid self-reinforcement. Science *372*, 1078–1081. https://doi.org/10.1126/science.aaz6694.

16. Jiang, L., Liu, C., Mayumi, K., Kato, K., Yokoyama, H., and Ito, K. (2018). Highly stretchable and instantly recoverable slide-ring gels consisting of enzymatically synthesized polyrotaxane with low host coverage. Chem. Mater. *30*, 5013–5019. https://doi.org/10.1021/acs.chemmater.8b01208.

17. Mayumi, K., Tezuka, M., Bando, A., and Ito, K. (2012). Mechanics of slide-ring gels: novel entropic elasticity of a topological network formed by ring and string. Soft Matter *8*, 8179–8183. https://doi.org/10.1039/c2sm25508a.

18. Choi, S., Kwon, T.W., Coskun, A., and Choi, J.W. (2017). Highly elastic binders integrating polyrotaxanes for silicon microparticle anodes in lithium ion batteries. Science *357*, 279–283. https://doi.org/10.1126/science.aal4373.

19. Gotoh, H., Liu, C., Imran, A.B., Hara, M., Seki, T., Mayumi, K., Ito, K., and Takeoka, Y. (2018). Optically transparent, high-toughness

elastomer using a polyrotaxane cross-linker as a molecular pulley. Sci. Adv. *4*, eaat7629. https://doi.org/10.1126/sciadv.aat7629.

20. Li, L., Lin, Q., Tang, M., Tsai, E.H.R., and Ke, C. (2021). An integrated design of a polypseudorotaxane-based sea cucumber mimic. Angew. Chem. Int. Ed. *60*, 10186–10193. https://doi.org/10.1002/anie.202017019.

21. Ito, K. (2012). Novel entropic elasticity of polymeric materials: why is slide-ring gel so soft? Polym. J. *44*, 38–41. https://doi.org/10.1038/pj.2011.85.

22. Jiang, Y., Zhang, Z., Wang, Y.X., Li, D., Coen, C.T., Hwaun, E., Chen, G., Wu, H.C., Zhong, D., Niu, S., et al. (2022). Topological supramolecular network enabled high-conductivity, stretchable organic bioelectronics. Science *375*, 1411–1417. https://doi.org/10.1126/science.abj7564.

23. Bin Imran, A., Esaki, K., Gotoh, H., Seki, T., Ito, K., Sakai, Y., and Takeoka, Y. (2014). Extremely stretchable thermosensitive hydrogels by introducing slide-ring polyrotaxane cross-linkers and ionic groups into the polymer network. Nat. Commun. *5*, 5124. https://doi.org/10.1038/ncomms6124.

24. Harada, A., Li, J., and Kamachi, M. (1994). Double-stranded inclusion complexes of cyclodextrin threaded on poly(ethylene glycol). Nature *370*, 126–128. https://doi.org/10.1038/370126a0.

25. Wenz, G., Han, B.H., and Müller, A. (2006). Cyclodextrin rotaxanes and polyrotaxanes. Chem. Rev. *106*, 782–817. https://doi.org/10.1021/cr970027+.

26. Uenuma, S., Maeda, R., Yokoyama, H., and Ito, K. (2019). Formation of well-defined supramolecular microstructures consisting of γ-cyclodextrin and polyether —rods, cubes, plates, and nanosheets—guided by guest polymer structure. Polymer *179*, 121689. https://doi.org/10.1016/j.polymer.2019.121689.

27. Ke, C., Yang, C., Mori, T., Wada, T., Liu, Y., and Inoue, Y. (2009). Catalytic enantiodifferentiating photocyclodimerization of 2-anthracenecarboxylic acid mediated by a non-sensitizing chiral metallosupramolecular host. Angew. Chem. Int. Ed. *48*, 6675–6677. https://doi.org/10.1002/anie.200902911.

28. Wang, H.M., and Wenz, G. (2011). Solubilization of polycyclic aromatics in water by γ-cyclodextrin derivatives. Chem. Asian J. *6*, 2390–2399. https://doi.org/10.1002/asia.201100217.

29. Jang, K., Iijima, K., Koyama, Y., Uchida, S., Asai, S., and Takata, T. (2017). Synthesis and properties of rotaxane-cross-linked polymers using a double-stranded γ-CD-based inclusion complex as a supramolecular cross-linker. Polymer *128*, 379–385. https://doi.org/10.1016/j.polymer.2017.01.062.

30. Iijima, K., Aoki, D., Otsuka, H., and Takata, T. (2017). Synthesis of rotaxane cross-linked polymers with supramolecular cross-linkers based on γ-CD and PTHF macromonomers: the effect of the macromonomer structure on the polymer properties. Polymer *128*, 392–396. https://doi.org/10.1016/j.polymer.2017.01.024.

31. Kureha, T., Aoki, D., Hiroshige, S., Iijima, K., Aoki, D., Takata, T., and Suzuki, D. (2017). Decoupled thermo- and pH-responsive hydrogel microspheres cross-linked by rotaxane networks. Angew. Chem. Int. Ed. *56*, 15393–15396. https://doi.org/10.1002/anie.201709633.

32. Hart, L.F., Lenart, W.R., Hertzog, J.E., Oh, J., Turner, W.R., Dennis, J.M., and Rowan, S.J. (2023). Doubly threaded slide-ring polycatenane networks. J. Am. Chem. Soc. *145*, 12315–12323. https://doi.org/10.1021/jacs.3c02837.

33. Tanaka, A., Kato, K., Ito, K., and Urayama, K. (2018). Pronounced effects of the densities of threaded rings on the strain-dependent Poisson's ratio of polyrotaxane gels with movable cross-links. Soft Matter *14*, 2808–2815. https://doi.org/10.1039/C8SM00257F.

34. To simplify the binding model, we assumed that a guest dimer is included in the cavities of two γ-CDs sequentially.

35. Lin, Q., Li, L., Tang, M., Uenuma, S., Samanta, J., Li, S., Jiang, X., Zou, L., Ito, K., and Ke, C. (2021). Kinetic trapping of 3D-printable cyclodextrin-based poly(pseudo)rotaxane networks. Chem *7*, 2442–2459. https://doi.org/10.1016/j.chempr.2021.06.004.

36. Lin, Q., Hou, X., and Ke, C. (2017). Ring shuttling controls macroscopic motion in a three-dimensional printed polyrotaxane monolith. Angew. Chem. Int. Ed. *56*, 4452–4457. https://doi.org/10.1002/anie.201612440.

37. Patterson, A.L. (1939). The Scherrer formula for X-ray particle size determination. Phys. Rev. *56*, 978–982. https://doi.org/10.1103/PhysRev.56.978.

38. Murakami, T., Schmidt, B.V.K.J., Brown, H.R., and Hawker, C.J. (2015). One-pot "click" fabrication of slide-ring gels. Macromolecules *48*, 7774–7781. https://doi.org/10.1021/acs.macromol.5b01713.

39. Murakami, T., Schmidt, B.V.K.J., Brown, H.R., and Hawker, C.J. (2017). Structural versatility in slide-ring gels: influence of co-threaded cyclodextrin spacers. J. Polym. Sci. Part A: Polym. Chem. *55*, 1156–1165. https://doi.org/10.1002/pola.28490.

40. Li, X., Maffettone, P.M., Che, Y., Liu, T., Chen, L., and Cooper, A.I. (2021). Combining machine learning and high-throughput experimentation to discover photocatalytically active organic molecules. Chem. Sci. *12*, 10742–10754. https://doi.org/10.1039/D1SC02150H.

41. Sui, F., Guo, R., Zhang, Z., Gu, G.X., and Lin, L. (2021). Deep reinforcement learning for digital materials design. ACS Materials Lett. *3*, 1433–1439. https://doi.org/10.1021/acsmaterialslett.1c00390.

42. Reis, M., Gusev, F., Taylor, N.G., Chung, S.H., Verber, M.D., Lee, Y.Z., Isayev, O., and Leibfarth, F.A. (2021). Machine-learning-guided discovery of 19F MRI agents enabled by automated copolymer synthesis. J. Am. Chem. Soc. *143*, 17677–17689. https://doi.org/10.1021/jacs.1c08181.

43. Pyzer-Knapp, E.O., Chen, L., Day, G.M., and Cooper, A.I. (2021). Accelerating computational discovery of porous solids through improved navigation of energy-structure-function maps. Sci. Adv. *7*, eabi4763. https://doi.org/10.1126/sciadv.abi4763.

44. Xie, T., France-Lanord, A., Wang, Y., Lopez, J., Stolberg, M.A., Hill, M., Leverick, G.M., Gomez-Bombarelli, R., Johnson, J.A., Shao-Horn, Y., et al. (2022). Accelerating amorphous polymer electrolyte screening by learning to reduce errors in molecular dynamics simulated properties. Nat. Commun. *13*, 3415. https://doi.org/10.1038/s41467-022-30994-1.

45. Nistanaki, S.K., Williams, C.G., Wigman, B., Wong, J.J., Haas, B.C., Popov, S., Werth, J., Sigman, M.S., Houk, K.N., and Nelson, H.M. (2022). Catalytic asymmetric C–H insertion reactions of vinyl carbocations. Science *378*, 1085–1091. https://doi.org/10.1126/science.ade5320.

46. Samha, M.H., Wahlman, J.L.H., Read, J.A., Werth, J., Jacobsen, E.N., and Sigman, M.S. (2022). Exploring structure-function relationships of aryl pyrrolidine-based hydrogen-bond donors in asymmetric catalysis using data-driven techniques. ACS Catal. *12*, 14836–14845. https://doi.org/10.1021/acscatal.2c04824.

47. We used the rates of the co-monomers' polymerizations in water at room temperature in a logarithmic scale (lnk) as their correspondent molecular descriptors in the models.

48. Lei, Z., Wang, Q., Sun, S., Zhu, W., and Wu, P. (2017). A bioinspired mineral hydrogel as a self-healable, mechanically adaptable ionic skin for highly sensitive pressure sensing. Adv. Mater. *29*, 1700321. https://doi.org/10.1002/adma.201700321.

49. Wang, Y., Zhang, L., and Lu, A. (2020). Highly stretchable, transparent cellulose/PVA composite hydrogel for multiple sensing and triboelectric nanogenerators. J. Mater. Chem. A *8*, 13935–13941. https://doi.org/10.1039/D0TA02010A.

50. Lei, Z., and Wu, P. (2018). Zwitterionic skins with a wide scope of customizable functionalities. ACS Nano *12*, 12860–12868. https://doi.org/10.1021/acsnano.8b08062.

51. Yin, M.-J., Yin, Z., Zhang, Y., Zheng, Q., and Zhang, A.P. (2019). Micropatterned elastic ionic polyacrylamide hydrogel for low-voltage capacitive and organic thin-film transistor pressure sensors. Nano Energy *58*, 96–104. https://doi.org/10.1016/j.nanoen.2019.01.032.

52. Huang, Z., Chen, X., O'Neill, S.J.K., Wu, G., Whitaker, D.J., Li, J., McCune, J.A., and Scherman, O.A. (2022). Highly compressible glass-like supramolecular polymer networks. Nat. Mater. *21*, 103–109. https://doi.org/10.1038/s41563-021-01124-x.

53. Nie, K., Wang, Z., Tang, R., Zheng, L., Li, C., Shen, X., and Sun, Q. (2020). Anisotropic, Flexible wood hydrogels and wrinkled, electrodeposited film electrodes for highly sensitive, wide-range pressure

sensing. ACS Appl. Mater. Interfaces *12*, 43024–43031. https://doi.org/10.1021/acsami.0c13962.

54. Shen, X., Nie, K., Zheng, L., Wang, Z., Wang, Z., Li, S., Jin, C., and Sun, Q. (2020). Muscle-inspired capacitive tactile sensors with superior sensitivity in an ultra-wide stress range. J. Mater. Chem. C *8*, 5913–5922. https://doi.org/10.1039/D0TC00453G.

55. Zhou, H., Wang, M., Jin, X., Liu, H., Lai, J., Du, H., Chen, W., and Ma, A. (2021). Capacitive pressure sensors containing reliefs on solution-processable hydrogel electrodes. ACS Appl. Mater. Interfaces *13*, 1441–1451. https://doi.org/10.1021/acsami.0c18355.

56. Zhu, Y., Lu, W., Guo, Y., Chen, Y., Wu, Y., and Lu, H. (2018). Biocompatible, stretchable and mineral PVA–gelatin–nHAP hydrogel for highly sensitive pressure sensors. RSC Adv. *8*, 36999–37007. https://doi.org/10.1039/C8RA06193A.

57. Zhang, Z., Tang, L., Chen, C., Yu, H., Bai, H., Wang, L., Qin, M., Feng, Y., and Feng, W. (2021). Liquid metal-created macroporous composite hydrogels with self-healing ability and multiple sensations as artificial flexible sensors. J. Mater. Chem. A *9*, 875–883. https://doi.org/10.1039/D0TA09730F.